Supplementary Figure 1

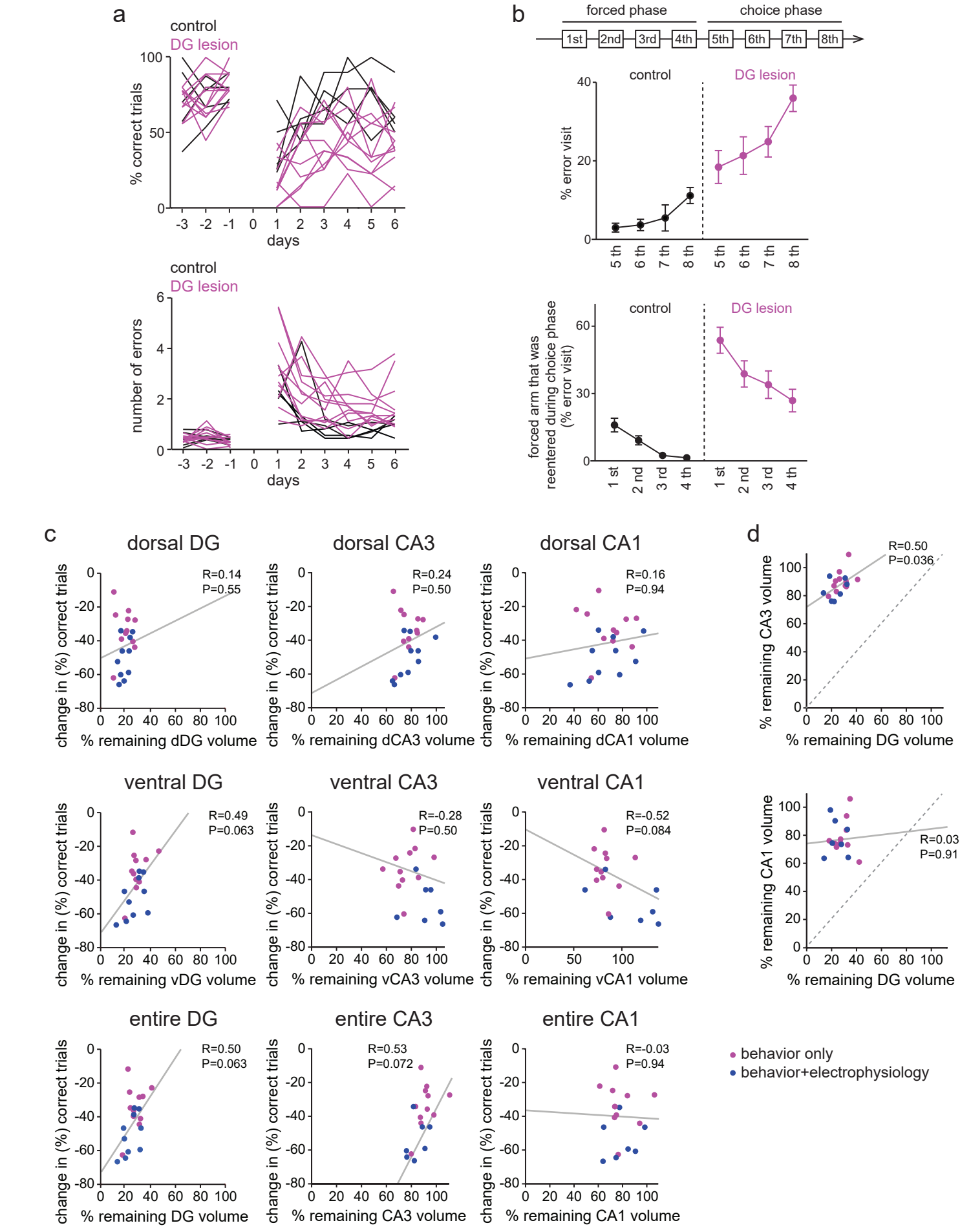

Supplementary Figure 1 Impaired behavioral performance was observed in all dentate gyrus lesioned animals. (**a**) Percent correct trials (top) and the mean number of errors per trial (bottom) during the days before surgery (-3 to -1) and after recovery from surgery (1 to 6) [n = 5 control and 11 dentate gyrus (DG)-lesioned animals, % correct trials: $F(1,70) = 16.07$, $P = 1.3 \times 10^{-3}$; number of errors: $F(1,70) = 6.55$, $P = 0.023$, repeated measures ANOVA over six days after surgery]. A trial was correct when each arm was only entered once, and each reentry into an arm that was previously visited within the trial was counted as an error. Each rat is represented by a single line (DG lesion, purple; control, black). (**b**) (Top) Percent repeat visits to a previously visited arm (error visits) during the trial are plotted by choice order. Errors occurred predominantly during later arm entries. (Bottom) Percent repeat visits (error visits) during the choice phase plotted by when in the forced phase the same arm was first visited. Incorrect arm entries in the choice phase occurred more frequently into arms that were visited early in the forced phase of the trial. Dashed lines separate control and lesioned group data. Lines and bars are mean ± SEM. (**c**) Percent correct performance against spared percent volume of the DG, CA3, and CA1 cell layers in DG-lesioned animals. Data are presented separately for dorsal regions, ventral regions, and the total area of each brain region. R values are calculated using a two tailed Pearson's correlation, and P values of correlations are Holm-Bonferroni corrected because volume measurements for these three conditions are in part overlapping. Each dot represents data from one animal. The data include animals used for behavioral experiments only [purple; n = 11 DG-lesioned animals, which are also shown in (a)] and animals used for electrophysiological experiments (blue; n = 10 DG-lesioned animals, **Supplementary Figure 10**). Volumes of cell layers were measured in cresyl violet-positive or NeuN-positive sections throughout the entire dorsoventral extent with computer-based 3-D volumetry (see Online Methods). For individual regions and DG-lesioned animals, the cell volume was normalized to the average of controls. (**d**) Percent total volume of the CA3 (top) and CA1 (bottom) cell layers against that of the DG cell layer in each DG-lesioned animal. Selective lesion of dentate granule neurons by colchicine injections into the DG caused minimal damage to CA1 and CA3 subfields, in comparison to DG.

Supplementary Figure 2

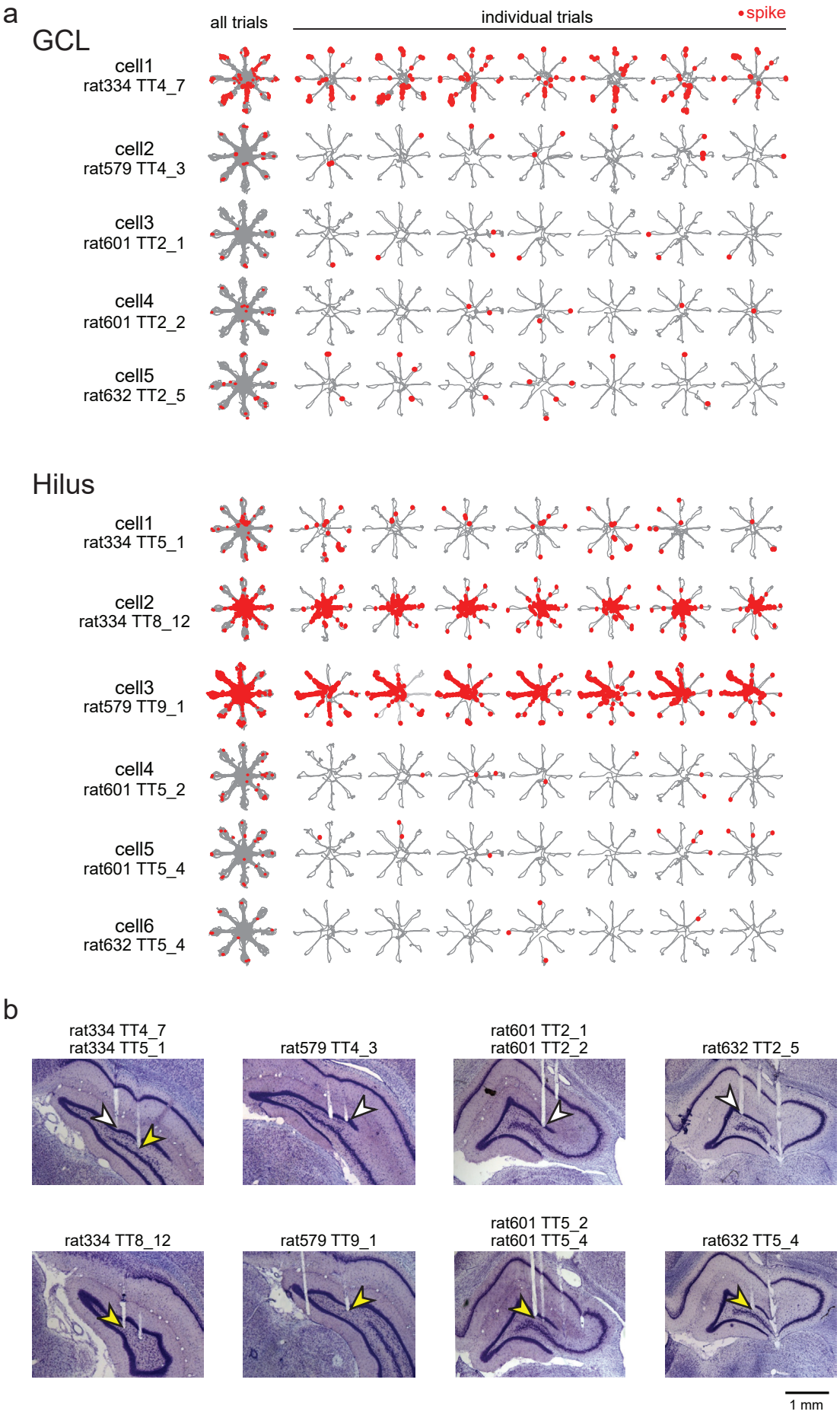

Supplementary Figure 2 Neuronal firing patterns of dentate cells in the working memory task. (**a**) Additional examples from cells on tetrodes located in the granule cell layer (GCL) (top) or the hilus (bottom) of the dentate gyrus. Each row depicts firing patterns of a single dentate neuron with the rat number, tetrode number, and cell number listed and the trajectories (gray) with spike locations (red dots) shown superimposed for all 20 trials in a recording session and separately for the first 7 of 20 trials (from left the right). Note that the majority of active dentate neurons preferentially fired action potentials at the end of the arm where reward was placed. The activity patterns of a smaller proportion of recorded cells corresponded to those of classic place cells, and these standard spatial firing patterns were more frequently observed for neurons recorded in the hilus (see **Fig. 2e**). (**b**) Histological confirmation of recording sites in cresyl-stained sections of the hippocampus for 4 different rats (left to right). Tetrode locations in the GCL are marked by white arrows and those in the hilus by yellow arrows. The rat number, tetrode number and cell number corresponding to each highlighted recording site is listed above each image for comparison to cells shown in (a).

Supplementary Figure 3

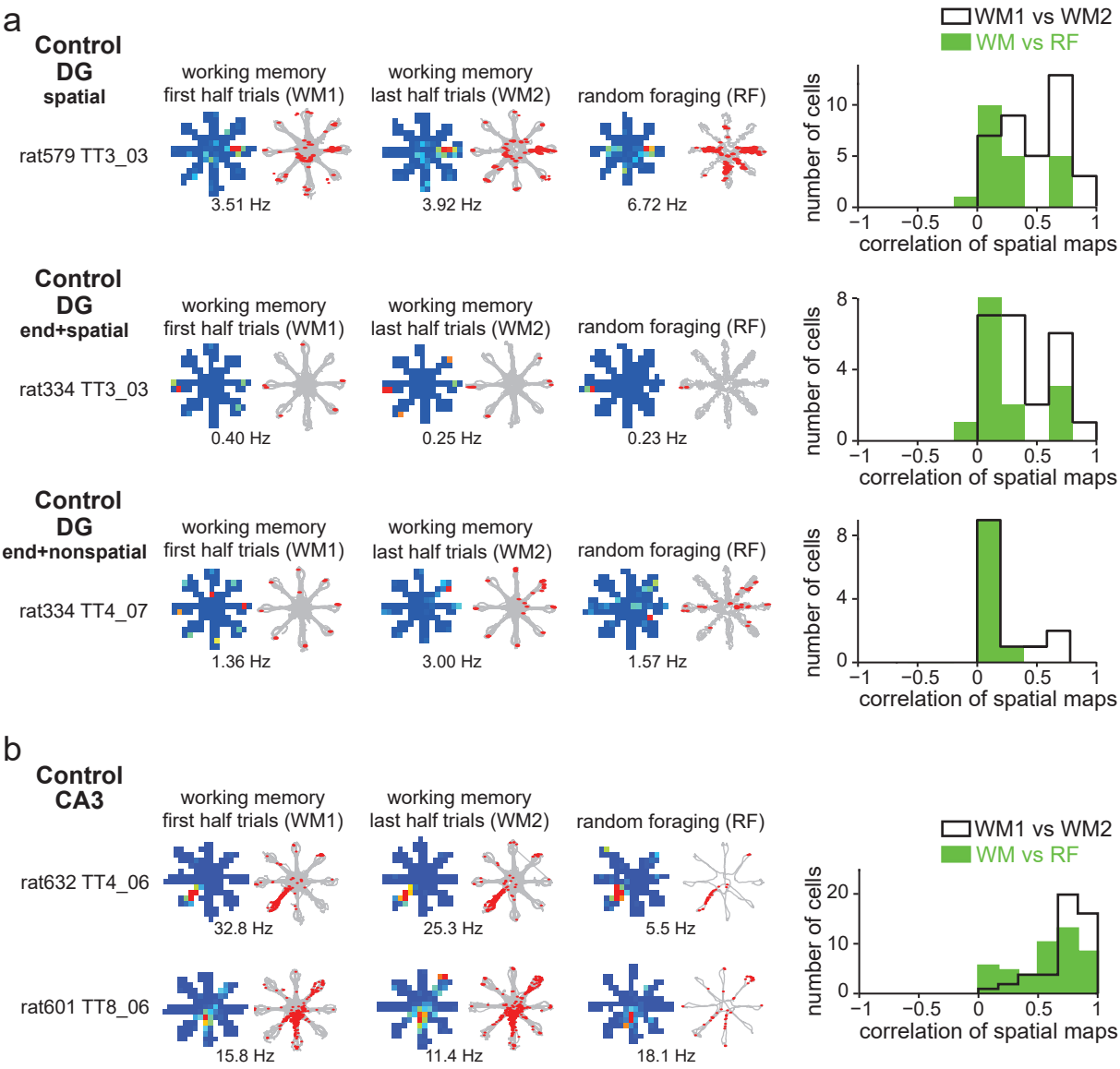

Supplementary Figure 3 Spatial firing patterns of dentate cells but not CA3 cells were task dependent. (**a**) (Left) Place-specific firing of 3 representative dentate cells in the working memory (WM) task and in the random foraging (RF) task. For each neuron, rate maps (blue, no firing; red, peak firing rate, as listed in Hz at the lower-right corner of each rate map) and trajectories with spike locations (red dots) are shown for the first and second half of WM trials (average duration of first half: 742 ± 62 s; second half: 820 ± 88 s) and for random foraging (RF, task duration = 600 s). The DG cells were classified based on firing patterns observed in the WM task, and for each DG cell class (spatial, end+spatial, nonspatial), spatial correlations between the first half and the second half of the WM task (white bars) and between the full duration of the WM task and the RF task (green bars) are shown. A spatial correlation of 1 indicates spatial maps that are identical, whereas 0 indicates uncorrelated spatial maps (spatial: WM1 vs WM2, n = 37 cells; WM vs RF, n = 21 cells. end+spatial: WM1 vs WM2, n = 23 cells; WM vs RF, n = 14 cells. end+nonspatial: WM1 vs WM2, n = 13 cells; WM vs RF, n = 10 cells). Note that the two spatial cell classes show corresponding maps within the WM task, but not between WM and RF. (**b**) Same as in (a), but for CA3 cells (*n* = 65 cells). CA3 neurons retain stable spatial maps in the radial arm maze irrespective of the task contingencies.

Supplementary Figure 4

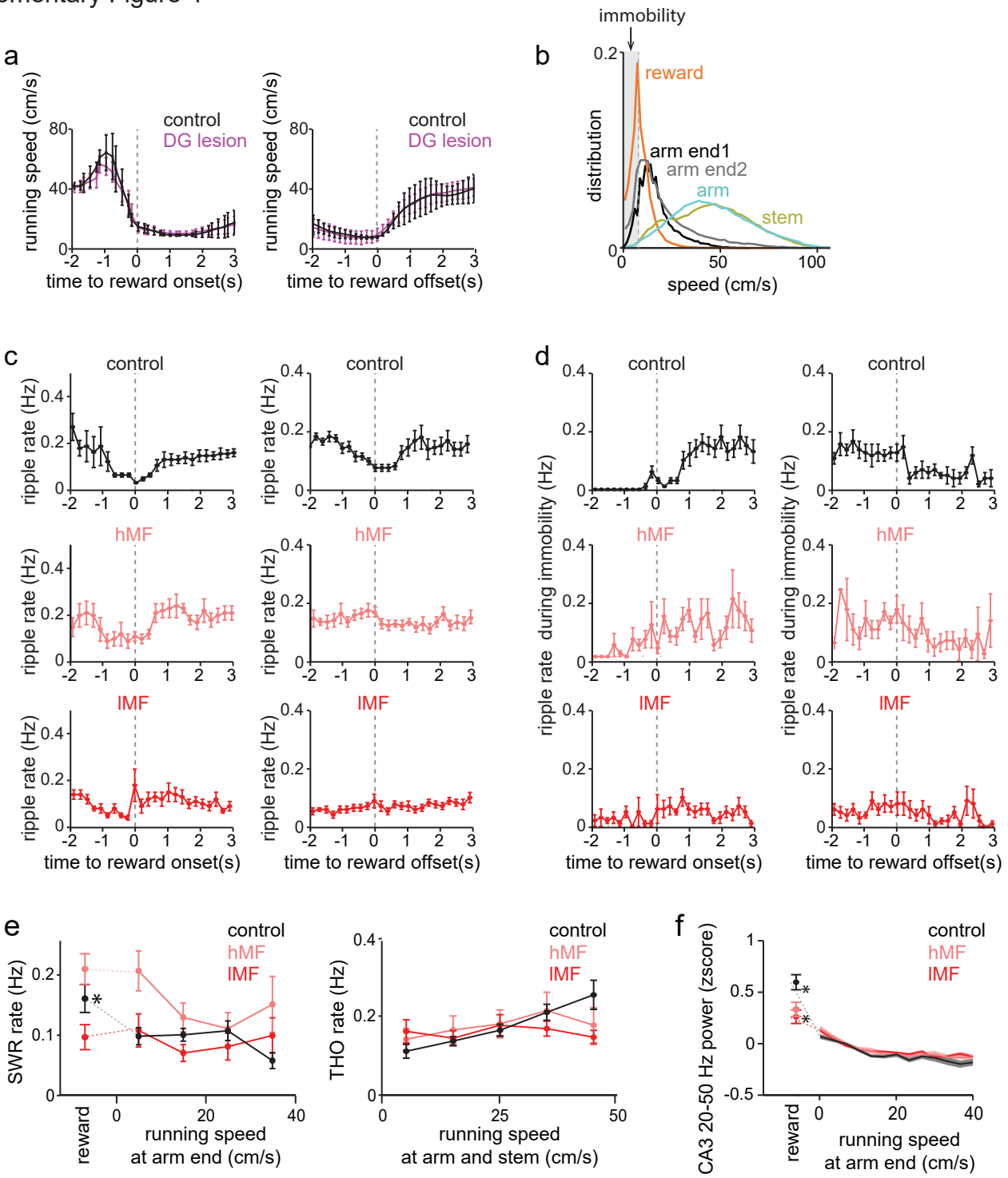

Supplementary Figure 4 Running speed and ripple rates relative to reward onset and offset. (**a**) Average running speed aligned to the onset (left) and offset (right) of reward consumption. (**b**) Distribution of running speed in each phase of behavior (n = 4 control and 10 DG lesion animals). Running speed of less than 10 cm/s was defined as immobility (indicated by dashed gray line). (**c**) CA3 ripple rates aligned to the onset and offset of reward consumption in control, high mossy fiber (hMF), and low mossy fiber (lMF) groups. All detected ripple events irrespective of running speed were included. Most ripple events before and after reward consumption represent movement-related high frequency oscillations detected at arms or the stem. (**d**) Same as in (c) but plotted for ripple events specifically detected during periods of immobility. The control group shows a prominent increase in immobility-associated ripples compared to the lMF group. Reward-associated ripples were infrequent immediately after the initial contact with the reward but incidence rates progressively increased with continued immobility at the reward location [for (c-f), control: n = 17 tetrodes (TT) from 4 animals; hMF: n = 10 TT from 5 animals;

Supplementary Figure 4

lMF: n = 20 TT from 9 animals]. (**e**) CA3 ripple rates are plotted against movement velocity and, on the left, separately for the period of reward consumption. Ripple event rates during reward exceeded the level that was observed when animals simply stopped without receiving reward in the control group [n = 17, 10, and 20 TT in control, hMF, lMF animals, respectively; two-sided paired t-test within group, control: t(16) = 4.14, $P = 8.3 \times 10^{-4}$; hMF: t(9) = 0.13, $P = 0.90$; lMF: t(19) = 1.00, $P = 0.33$]. * $P < 0.05$ for reward-related compared to general immobility. (**f**) CA3 20-50 Hz power is plotted against movement velocity and separately for periods of reward consumption. Although the oscillations had higher power during immobility compared to running (repeated measures ANOVA, control: F(25,400) = 13.85, $P < 10^{-10}$; hMF: F(25,225) = 6.14, $P = 1.9 \times 10^{-5}$; lMF: F(25,475) = 8.92, $P < 10^{-10}$), 20-50 Hz power during reward-related immobility even exceeded the level that was observed when animals simply stopped without receiving reward [two-sided paired t-test within group, control: t(16) = 8.91, $P = 5.8 \times 10^{-8}$; hMF: t(9) = 2.85, $P = 0.019$; lMF: t(19) = 2.22, $P = 0.038$]. Compared to controls, DG lesions reduced 20-50 Hz power during reward consumption [control vs hMF: t(25) = 3.08, $P = 0.010$; control vs lMF: t(35) = 3.66, $P = 0.0017$]. * $P < 0.05$ for reward-related compared to general immobility. Dashed lines in (a)(c)(d) denote reward consumption at time 0. Symbols with bars are mean ± SEM.

Supplementary Figure 5

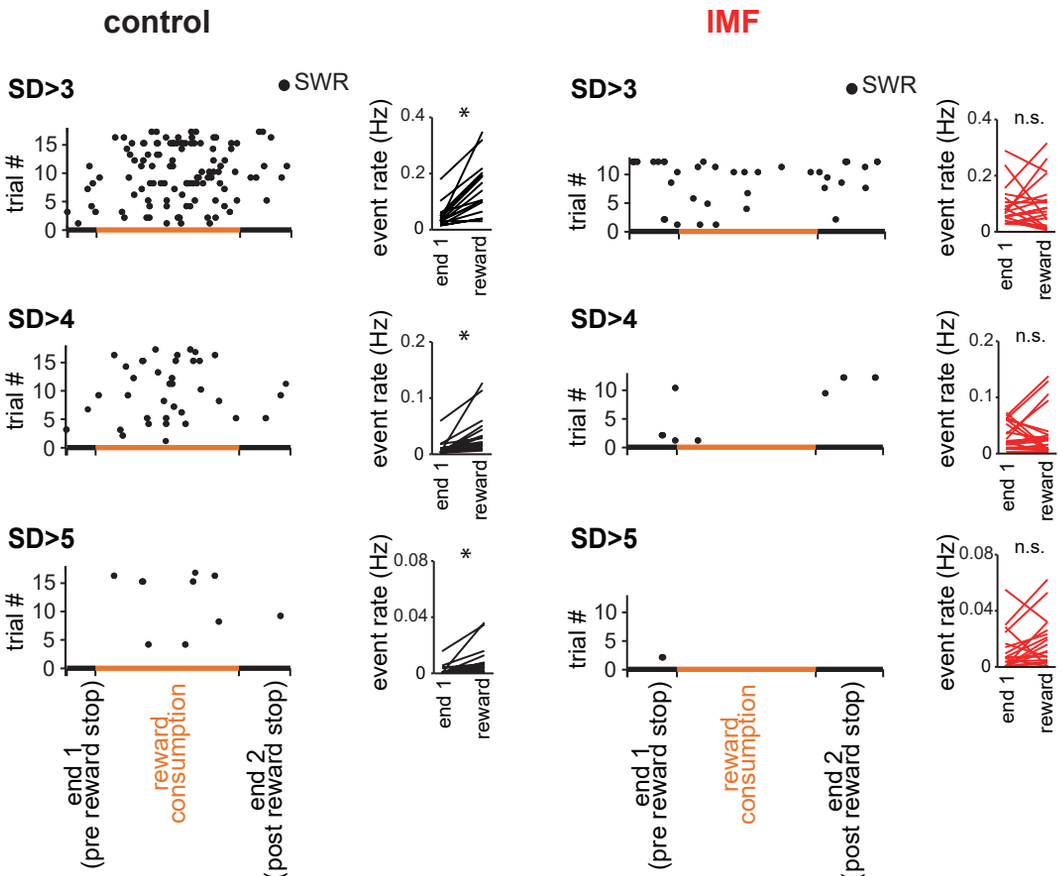

Supplementary Figure 5 CA3 SWRs at different thresholds. Example rastergrams show the distribution of CA3 SWR events that were detected with different criteria (threshold of 3, 4, and 5 SD above the mean). Events at a control recording site and at a low-density mossy fiber (lMF) recording site are plotted as described in **Fig. 3g** (control: n = 17 tetrodes from 4 animals; lMF: n = 20 tetrodes from 9 animals). Incidence rates of ripple events detected at different thresholds (3, 4 and 5 SD) and during different behavioral periods are shown to the right of the example rastergrams. Each line represents a tetrode. In the control group, the rates of SWRs were significantly higher during reward consumption compared to before contact with the reward (arm end 1) for all ripple thresholds [n = 17 tetrodes; SD > 3: t(16) = 5.76, $P = 2.9 \times 10^{-5}$; SD > 4: t(16) = 3.73, P = 0.0018; SD > 5: t(16) = 3.53, P = 0.0028, two-sided paired t-test]. In the lMF group, the rates of SWRs were not significantly different between immobility before reward (arm end 1) and reward for any of the thresholds [n = 20 tetrodes, two-sided paired t-test; SD > 3: t(19) = 0.38, P = 0.70; SD > 4: t(19) = 0.39, P = 0.70; SD > 5: t(19) = 0.46, P = 0.65]. * $P < 0.05$

Supplementary Figure 6

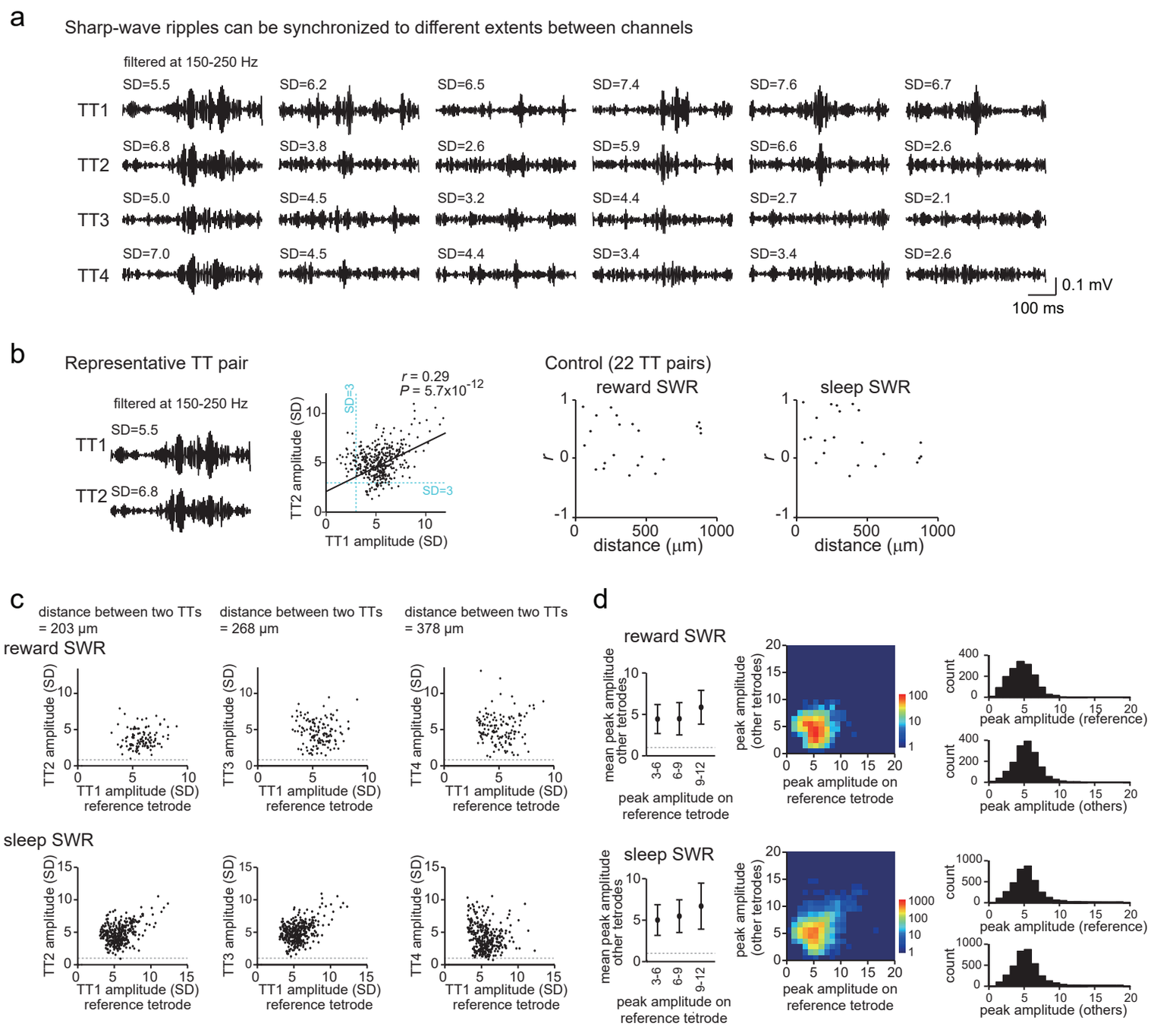

Supplementary Figure 6 Coherence of SWR amplitudes across CA3 recording sites. (**a**) Band-pass (150-250 Hz) filtered LFP traces recorded from four sites (tetrode 1-4) in the hippocampal CA3 region of a control rat. The standard deviations (SD) of individual ripple events are shown to the top left of each LFP trace. The traces show simultaneous occurrence of ripples (SD > 3) on all tetrodes (TTs), on two TTs, and on a single TT, confirming many instances in which SWRs were detected on different subsets of electrodes. (**b**) To quantify to what extent ripple amplitudes differed across recording sites, SD values of ripple events were compared between pairs of CA3 recording sites (n = 3025 ripple events). Left, example ripple event on two recording sites (TT1, TT2). Right, each dot is a ripple event and the *r* value quantifies whether ripple amplitude was corresponding across the two recording sites. The *r* values for all pairs of recording sites (*n* = 22 pairs from 4 control animals) are plotted against the distance between the sites (two-sided Pearson's correlation). By separately analyzing SWRs at reward locations and SWRs during sleep, we controlled for movement-related noise. Noise artifacts during movement would be expected to generate events with similar amplitude across recording sites and therefore increase correlations between sites. The similar distribution of correlation coefficients confirms that noise correlations did not compromise signal quality

Supplementary Figure 6

during movement. Furthermore, although there was a trend for amplitudes on more distal sites to be less correlated, even SWRs at proximal sites could be uncorrelated. (**c**) Despite the low degree of pairwise correlations, there were on average high-amplitude signals (measured in standard deviations) on other tetrodes when a high-amplitude signal was detected on one tetrode, as shown in the example traces in (a) and (b, left) and in the scatterplots for reward and sleep SWRs from one example rat (20 trials, n = 185 ripple events). (**d**) Amplitude of all simultaneously recorded events are compared (n = 4 animals, 22 TT pairs). Left: the amplitude on other channels is shown for each range of amplitudes on a reference channel. Center: Color-coded density of the amplitude distribution between a reference channel and other channels. Right: Distribution of the amplitudes on a reference channel and on other channels. The pattern of results generally resembles those obtained in ref. 31 for CA1 but signals in CA3 appear more local than those in CA1. Symbols with bars are mean ± SEM.

Supplementary Figure 7

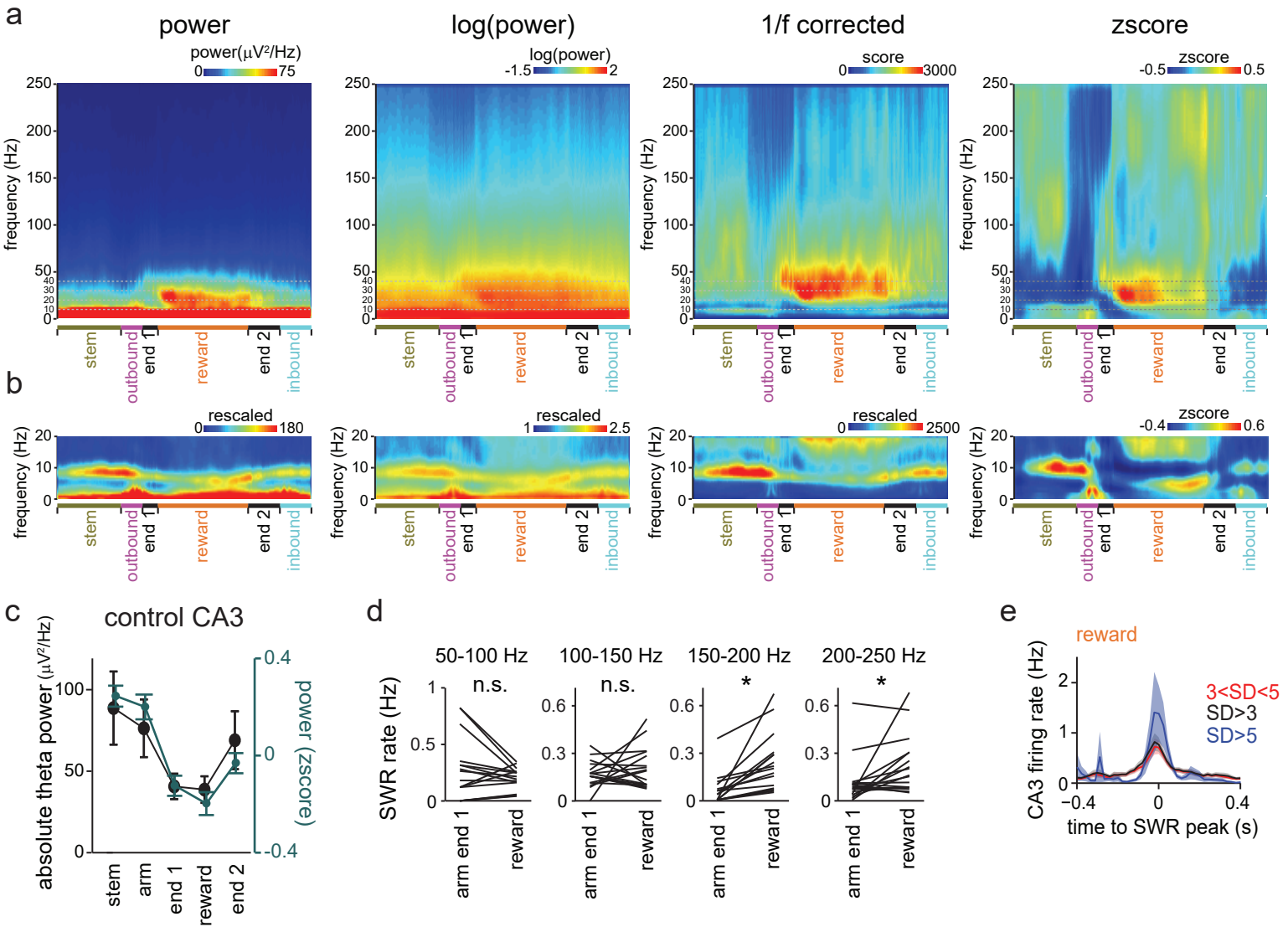

Supplementary Figure 7 Power and incidence of oscillatory events in different frequency bands. (**a**) Different normalization methods were applied to time-frequency spectra of the hippocampal CA3 LFP recordings shown in **Fig. 3e** (1 CA3 recording site, n = 18 trials). (Left to right) Raw power spectrogram, power spectrum on a logarithmic scale, 1/f-corrected power spectrum, and z-scored power spectrum. Z-scores were calculated over time within each frequency. The full range of LFP changes in the theta, 20-50 Hz, gamma, and ripple bands is only apparent in the z-scored spectrum, and we therefore used the z-score normalization to compare LFP signals on different recording electrodes. (**b**) Subplots that magnify the low frequency range (0-20 Hz) from each of the time-frequency spectra shown in (a). The color scale was adjusted from (a) to best visualize the theta band. (**c**) The average theta power without normalization (black) is plotted together with the average theta power after z-score renormalization (green, same as in **Fig. 5e**)(n = 17 tetrodes from 4 animals). Both analyses show a corresponding pattern of amplitudes across behavioral phases. (**d**) In individual frequency bands, LFP signals were band-pass filtered and events were detected when the root mean-square power of the filtered traces exceeded 3 standard deviations above the mean. Each line represents a tetrode (n = 17 tetrodes from 4 animals). The rate of events before (arm end 1) and during reward was significantly different for only the 150-200 Hz and 200-250 Hz bands [n = 17 tetrodes; 50-100 Hz: t(16) = 2.02, P = 0.064; 100-150 Hz: t(16) = 1.08, P = 0.29; 150-200 Hz: t(16) = 2.97, P = 0.0091; 200-250 Hz: t(16) = 2.26, P = 0.038, two-sided paired t test]. The selective differences of immobility-related oscillations in only the high-frequency bands further confirms that they correspond to standard SWRs. (**e**) Ripple-triggered firing rates of CA3 pyramidal cells for ripples detected at different thresholds (3 < SD, 3 < SD < 5 and SD < 5 above the mean). Symbols with bars in (c) and lines with shaded regions in (e) are mean ± SEM.

Supplementary Figure 8

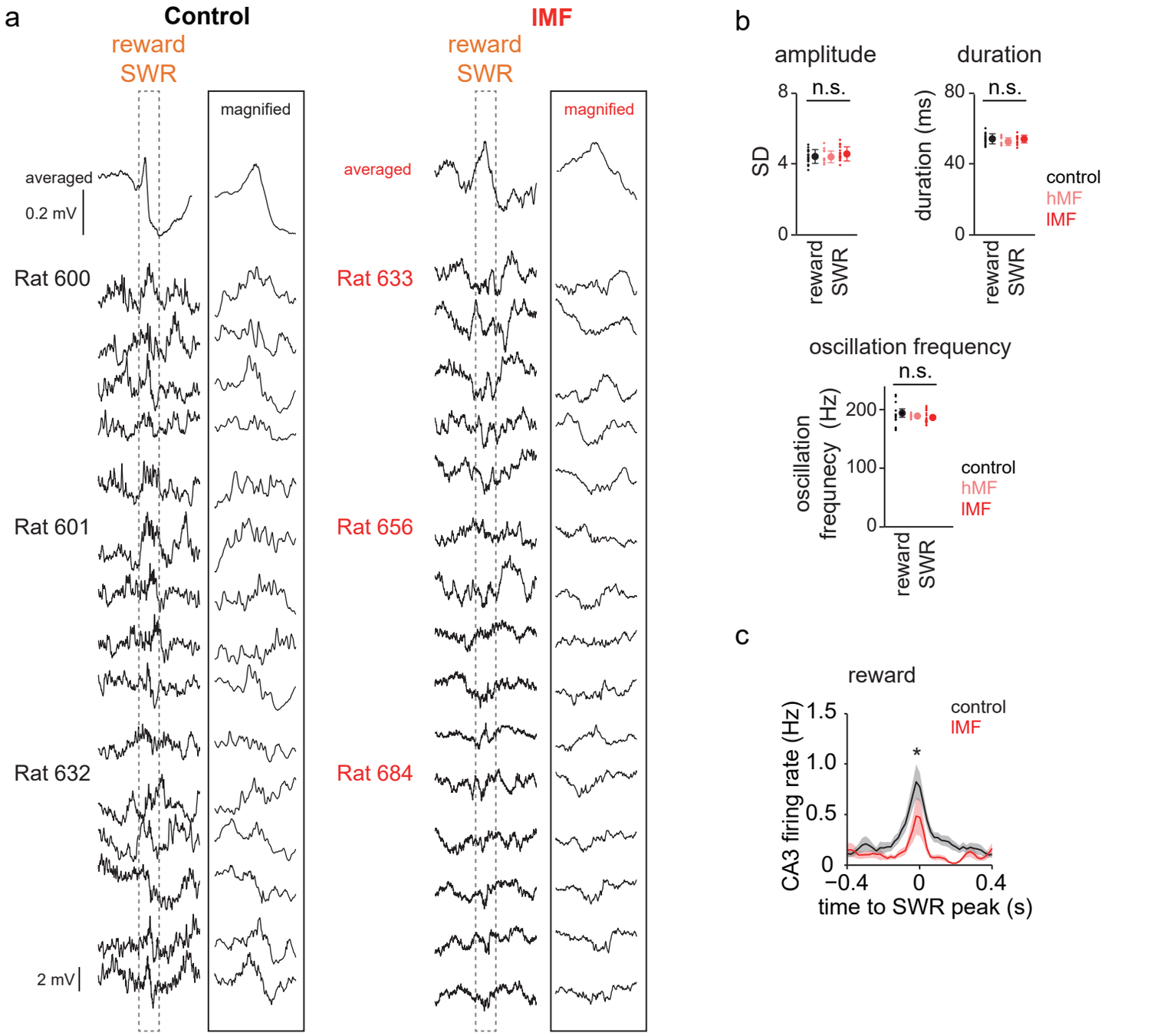

Supplementary Figure 8 Characterization of 150-250 Hz oscillations during reward. (**a**) Example LFP traces of SWR events that were recorded at control (left, black) and lMF sites (right, red) during spatial WM behavior. The peak-aligned average unfiltered LFP traces at the top of each panel are averages over all recorded events in the study while **Fig. 3f** shows an average for all events in one recording session. Examples of five individual raw LFP traces per animal are shown from three different animals per group). Magnified traces from the time period in the stippled box are shown to the right of each panel. (**b**) Comparison of ripple amplitude, duration and frequency. For SWRs at reward, z-scored amplitude (top left), duration (top right) and frequency (bottom) did not differ between recording sites in control animals, lMF sites in DG-lesioned animals, and high-density mossy fiber (hMF) sites in DG-lesioned animals [n = 17, 10, and 20 tetrodes in 4 control, 5 hMF, 9 lMF animals, respectively; z-scored amplitude of reward SWR: $F(2,45) = 1.48$, $P = 0.24$; $P = 0.15$; duration of reward SWR: $F(2,45) = 1.86$, $P = 0.17$, repeated measures ANOVA]. (**c**) Ripple-peak triggered firing rates of CA3 pyramidal cells. SWR-associated firing is DG dependent (n = 65 control cells, black; n = 44 cells at lMF sites in DG-lesioned rats, red) (control versus lMF at 0 s, U = 3624, Z = 2.37, $P = 0.018$, two-sided Mann-Whitney U test). *$P < 0.05$. Lines with shaded regions are mean ± SEM.

Supplementary Figure 9

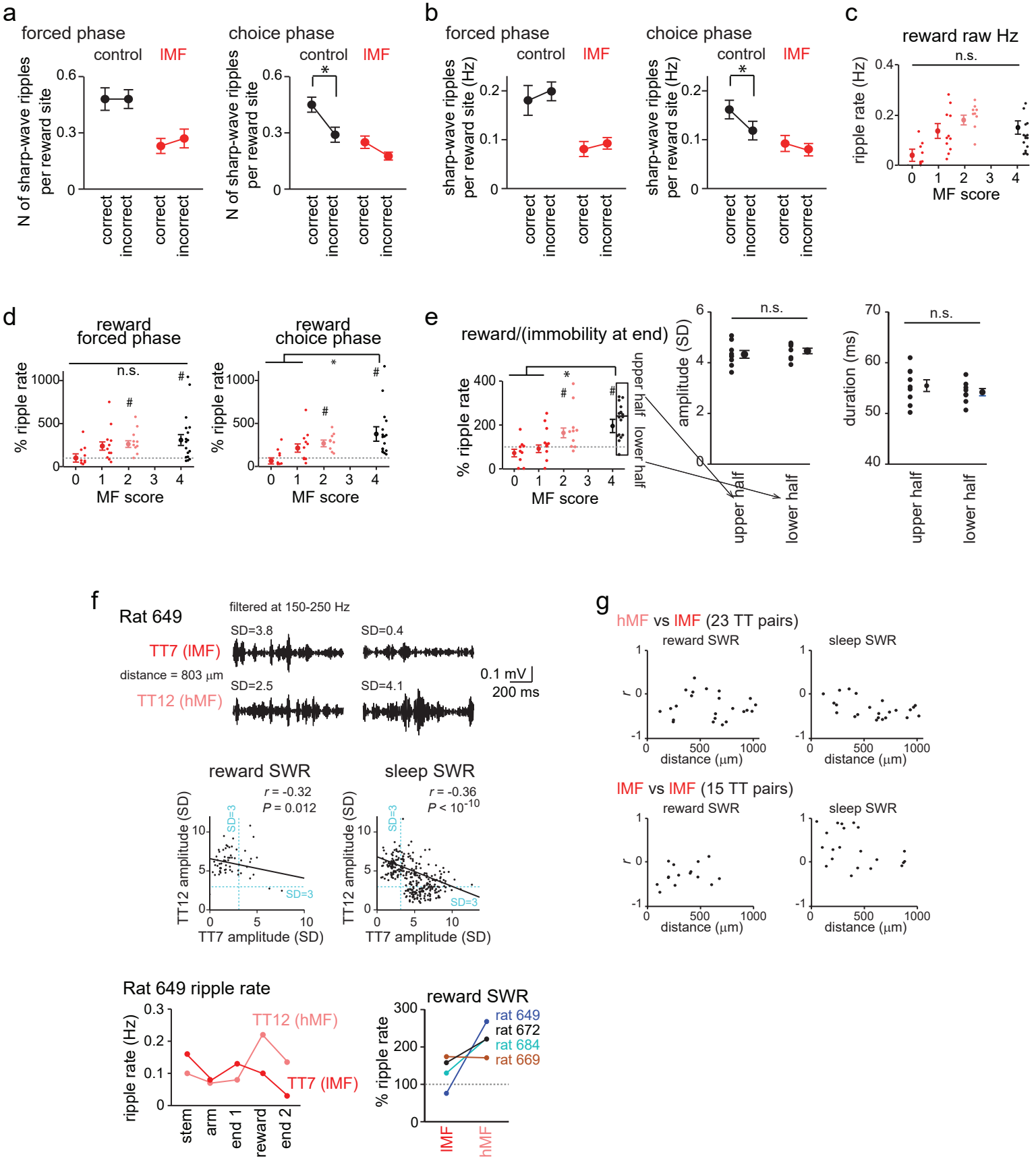

Supplementary Figure 9 Immobility-associated sharp-wave ripples in the working memory task. (**a**) Mean number of reward-associated sharp-wave ripples (SWRs) during the forced phase (left) and choice phase (right) at control sites [black, $n = 17$ tetrodes (TT)] and lMF sites (red, $n = 20$ TT) are compared between correct and incorrect trials [forced phase, control, $t(16) = 0.03$, $P = 0.97$; forced phase, lMF: $t(17) = 1.28$, $P = 0.22$; choice phase, control: $t(16) = 5.78$, $P = 2.8 \times 10^{-5}$; choice phase, lMF: $t(17) = 1.95$, $P = 0.068$, two-sided paired t test]. $^*P < 0.05$. Bars are mean ± SEM. (**b**) Same as (a) but for incidence rate [forced phase, control, $t(16) = 0.92$, $P = 0.37$; forced phase, lMF: $t(17) = 0.54$, $P = 0.60$; choice phase, control: $t(16) = 2.13$, $P = 0.049$; choice phase, lMF: $t(17) = 0.65$, $P = 0.53$, two-sided paired t test]. While a higher number of reward-related SWRs in correct compared to incorrect trials were detected at control CA3 sites during the choice phase, there was no difference in the ripple rate between correct and incorrect trials at the low-density MF sites, consistent with the notion that memory-related ripples are no longer sufficiently promoted with reduced DG input. $^*P < 0.05$. (**c**) Incidence rate of reward-associated CA3 SWR events, grouped by the MF score (score 0: $n = 9$ TT from 6 animals, score 1: n = 11 TT from 6 animals, score 2: n = 10 TT from 5 animals, score 4, control: n = 17 TT from 4 animals). The values for each recording site (dots with similar values jittered along the horizontal axis for visualization) and the mean (± SEM) for each group are shown. Raw rates during the reward period did not differ between groups (control vs lMF, U = 384, Z = 1.84, $P = 0.13$, two-sided Mann-Whitney U test; control vs hMF, U = 198, Z = 1.98, $P = 0.095$, two-sided Mann-Whitney U test). However, an increase in SWR rates during the reward period compared to immobility at arm ends was only observed for a MF score of 2 and not for scores of 0 and 1 [reward vs immobility at arm end period, score 0: reward, 0.042 ± 0.015 Hz, immobility at end, 0.057 ± 0.015 Hz, $t(8) = 1.38$, $P = 0.21$; score 1: reward, 0.140 ± 0.029 Hz, immobility at end, 0.129 ± 0.024 Hz, $t(10) = 0.43$, $P = 0.68$, reward vs immobility at arm end period, score 2: reward, 0.215 ± 0.024 Hz, immobility at end, 0.134 ± 0.017 Hz, $t(9) = 2.71$, $P = 0.024$; two-sided paired *t* test]. (**d**) (Left) Ripple rates during reward consumption in the forced phase, normalized to periods when the animal was stopped at the arm end before reward consumption. A significant increase was only observed for control and hMF sites [score 0: $t(8) = 0.23$, $P = 0.82$; score 1: $t(10) = 1.30$, $P = 0.22$; score 2; $t(9) = 4.28$, $P = 0.0020$; score 4; $t(16) = 2.84$, $P = 0.012$], but differences between control and DG-lesioned sites did not reach significance during the forced phase (two-sided paired *t* test; control vs lMF, U = 322, Z = 1.75, $P = 0.080$; control vs hMF, U = 145, Z = 0.233, $P = 0.82$, two-sided Mann-Whitney U test). # $P < 0.05$, two-sided paired *t* test within group. (Right) Same as the left panel but for the choice phase. A significant increase was only observed for control and hMF sites [score 0: $t(8) = 1.04$, $P = 0.33$; score 1: $t(10) = 0.63$, $P = 0.54$; score 2; $t(9) = 5.31$, $P = 4.9 \times 10^{-4}$; score 4; $t(16) = 3.89$, $P = 0.0013$], and the increase in ripple rate during reward consumption was significantly higher at control than at lMF sites (two-sided paired *t* test; control vs lMF, U = 423, Z = 3.03, $P = 0.0024$; control vs hMF, U = 245, Z = 0.33, $P = 0.74$, two-sided Mann-Whitney U test). $^*P < 0.05$, Mann-Whitney U test across the groups; # $P < 0.05$, paired *t* test within group. Statistics for the forced and choice phase combined are provided in the main text (**Fig. 4e**). (**e**) To determine whether SWRs with the most pronounced rate increase at reward locations differed from those that were less responsive, we compared the shape and amplitude of the SWRs in the lower and upper half of the range and found them to be indistinguishable [paired *t* test, amplitude: $t(15) = 0.68$, $P = 0.51$; duration: $t(15) = 0.90$, $P = 0.38$]. (**f**) Within-animal variability of CA3 ripple rate. In an animal with a colchicine lesion of dentate granule cells (rat 649), SWR rates were compared between CA3 tetrodes with high-density MF input (hMF; tetrode 12) or low-density MF input (lMF, tetrode 7). (Top) Examples of SWRs with an amplitude > 3 SD on only one of the two tetrodes. (Middle) Scatterplots show that reward SWRs (n = 62 events) occurred predominantly on the hMF tetrode while sleep SWRs (n = 303 events) could be detected at both tetrodes. The negative correlations between amplitudes at the two sites indicate that most SWRs were detected on either one or the other channel, as also shown in the examples on top (two-sided Pearson's correlation). (Bottom left) Only TT12 (hMF) shows an increase in the ripple rate specific to reward. (Bottom right) Comparison of average reward-triggered SWR rates between tetrodes with hMF input (MF score of 2, see Online Methods) and lMF input (MF scores of 0 and 1) in each DG-lesioned animal with both types of recording sites. (**g**) Quantification of SWR amplitudes across tetrode pairs. The correlation between all events on a tetrode pair was first calculated as in (f) and each correlation coefficient is then plotted against the pair's distance. Correlations between tetrode pairs were already low in controls (**Supplementary Fig. 6b**), and the even lower correlations in lesioned rats are consistent with the dependence of SWRs on the density of mossy fiber inputs (hMF vs lMF: n = 23 TT pairs from 4 animals, lMF vs lMF: 15 TT pairs from 8 animals).

Supplementary Figure 10

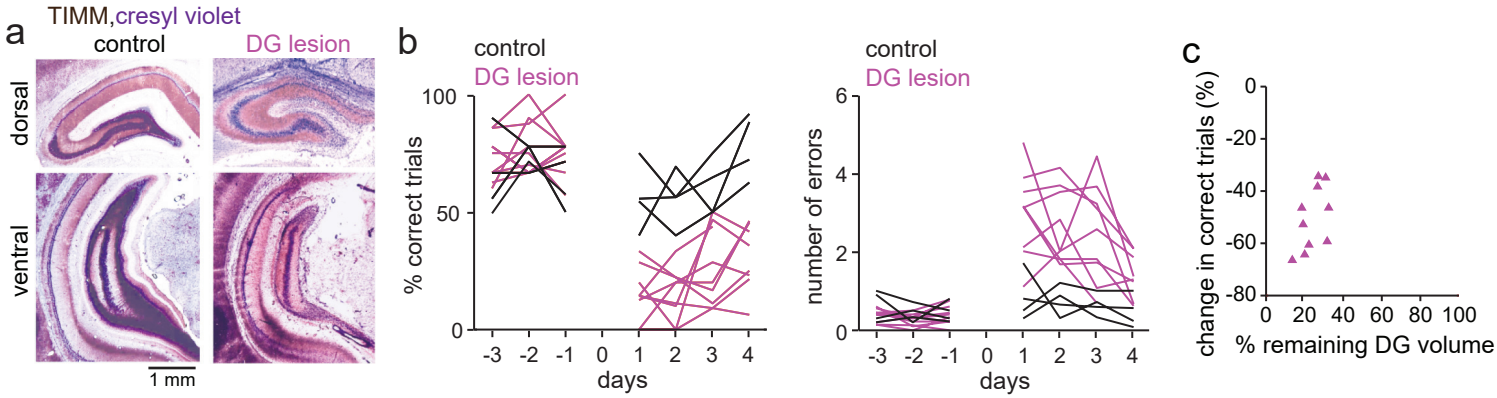

Supplementary Figure 10 Behavioral performance in animals used for electrophysiological experiments. (**a**) Coronal brain sections of the dorsal and ventral hippocampus. Cell bodies are labelled with cresyl violet (purple), and the mossy fibers (MF) of dentate granule cells are labelled with TIMM (black). (**b**) Percent correct trials (left) and the mean number of errors per trial (right) during the days before surgery (-3 to -1) and after recovery from surgery (1 to 4) (n = 4 control and 10 lesioned animals; control vs DG lesion, % correct trials: $F(1,36) = 68.65$, $P < 10^{-10}$; number of errors: $F(1,36) = 15.40$, $P = 0.0020$, repeated measures ANOVA over four days after surgery). Data is as shown in **Supplementary Fig. 1a**. Each rat is represented by a single line. (**c**) Relationship between percent spared DG volume and decrease in percent correct performance (compared to presurgical performance) in DG-lesioned animals. Data is plotted as shown in **Supplementary Fig. 1c**. Each dot represents data from one animal.

Supplementary Figure 11

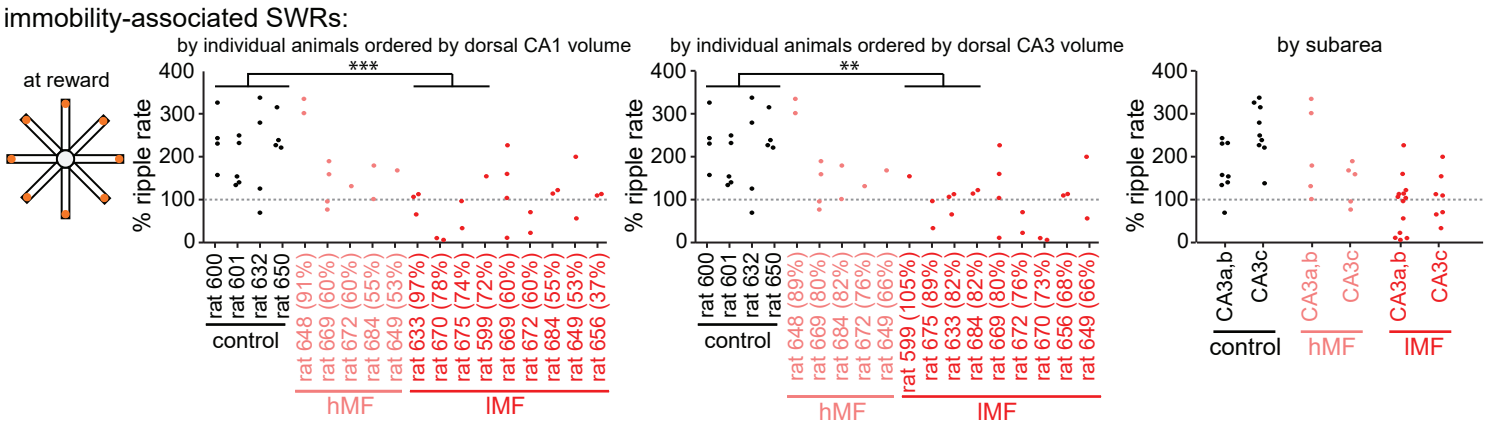

Supplementary Figure 11 Normalized incidence rates of reward SWRs (compared to immobility before reward) in the spatial WM task. Ripple rates at each recording site are ordered by remaining dorsal CA1 volume of each animal (left), by remaining dorsal CA3 volume (center), and by CA3 subareas (right). For visualization, data points with similar values were jittered along the horizontal axis. We found that mossy fiber density rather than a reduction in CA1 or CA3 volume was related to the reduction in immobility ripples. For example, SWR rates were reduced when comparing the CA3 recording sites (n = 17 tetrodes) of the 4 control animals to the lMF sites (n = 8 tetrodes) of either the 4 animals with least dorsal CA1 damage (U= 279, Z = 3.35, $P = 8.1 \times 10^{-44}$) or the four animals with the least dorsal CA3 damage (U = 277, Z = 3.29, $P = 0.0012$; two-sided Mann-Whitney test). Furthermore, regression analysis revealed no correlation between either CA1 or CA3 volume and SWR reduction (lMF sites, $n = 20$, CA1: r = 0.23, $P = 0.37$, CA3: r = 0.13, $P = 0.59$; lMF and hMF sites combined, $n = 30$, CA1: r = 0.02, $P = 0.45$, CA3: r = 0.27, $P = 0.15$). ** $P < 0.01$, *** $P < 0.001$

Supplementary Figure 12

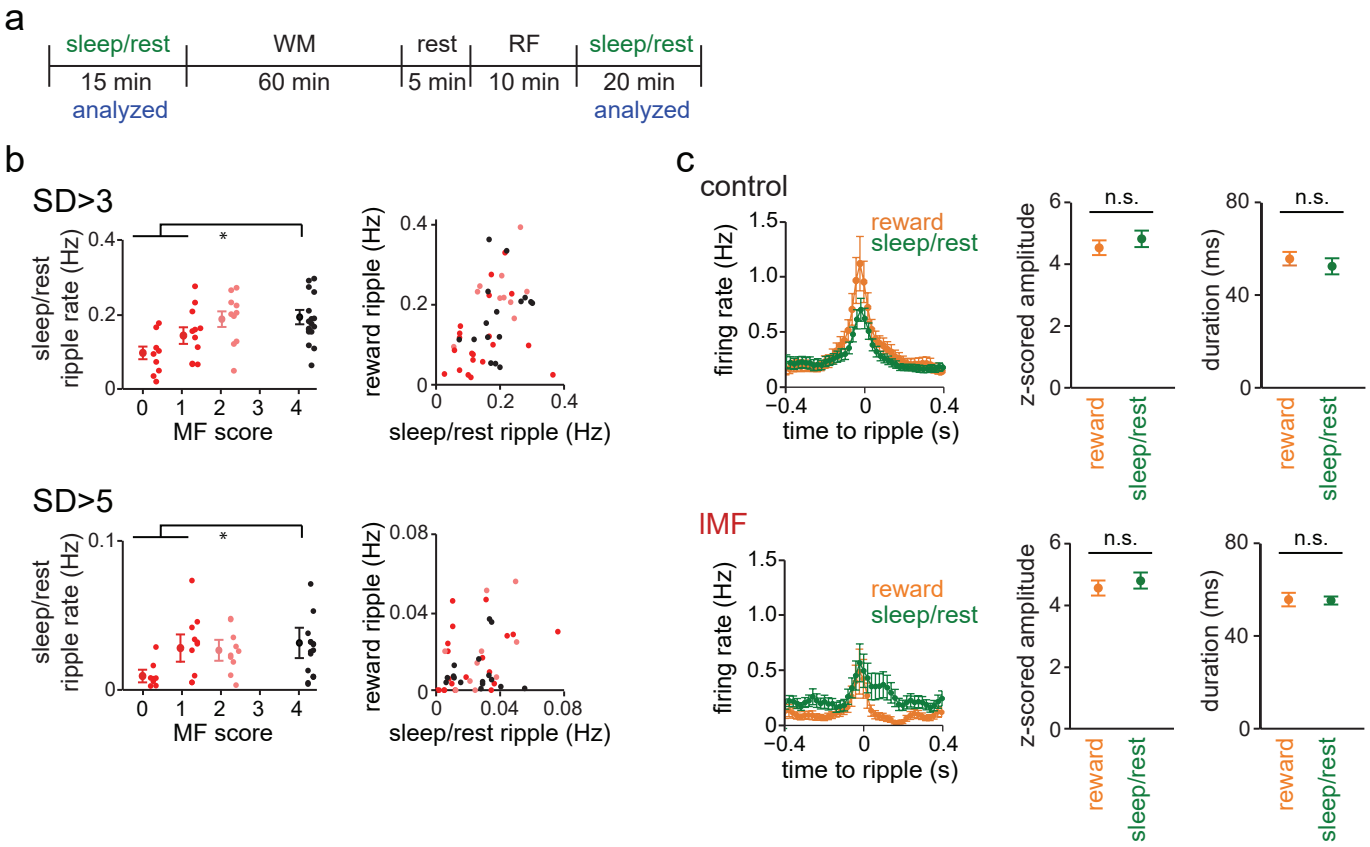

Supplementary Figure 12 CA3 sharp-wave ripple events during periods of sleep and rest depend on mossy fiber projections from dentate granule neurons. (**a**) Sleep/rest periods include 15-min sessions before the working memory (WM) task and 20-min sessions after the random foraging (RF) task while recordings were performed in a holding box. (**b**) (Left panels) Incidence rate of ripple events during the sleep/rest periods, grouped by the MF score (score 0: n = 9 TT from 6 animals, score 1: n = 11 TT from 6 animals, score 2: n = 10 TT from 5 animals, score 4, control: n = 17 TT from 4 animals). The values for each recording site (dots with similar values jittered along the horizontal axis for visualization) and the mean (± SEM) for each group are shown for two SWR thresholds. In rest/sleep, the difference in SWR rates at lMF compared to control sites reached significance only for the lower threshold (SD > 3; control vs lMF, U = 404, Z = 2.45, P = 0.028; control vs hMF, U = 228, Z = 0.48, P > 0.99, two-sided Mann-Whitney U test; SD > 5; control vs lMF, U = 302, Z = 2.36, P = 0.036; control vs hMF, U = 272, Z = 1.65, P = 0.20, two-sided Mann-Whitney U test). *P < 0.05, Mann-Whitney U test across groups. (Right panels) For the same recording sites, the relationship between the rates of sleep/rest ripple events and the rates of reward-associated ripple events during WM are shown (SD > 3, R = 0.55, $P = 6.9 \times 10^{-5}$; SD > 5, R = 0.20, P = 0.19). These results indicate that CA3 ripple events during sleep/rest periods also depend on MF input and that DG input is necessary for supporting immobility-related ripples in awake-behavior and sleep/rest. (**c**) (Left) Ripple-triggered changes in firing rates of CA3 pyramidal cells are compared for SWRs in sleep/rest (green) and during reward consumption (orange). In sleep/rest as well as in reward periods, the firing rate of individual CA3 cells increased several-fold from low baseline levels. (Right) Comparison of ripple amplitude and duration between sleep/rest and reward consumption. For control and lMF groups, z-scored ripple amplitude and duration did not differ between sleep/rest and reward periods [n = 17 and 20 TT in 4 control and 9 lMF animals, respectively; z-scored amplitude of control: t(16) = 1.42, P = 0.18; z-scored amplitude of lMF: t(19) = 0.62, P = 0.54; duration of control: t(16) = 0.55, P = 0.59; duration of lMF: t(19) = 0.99, P = 0.34; two-sided paired t test]. Symbols with bars are mean ± SEM.

Supplementary Figure 13

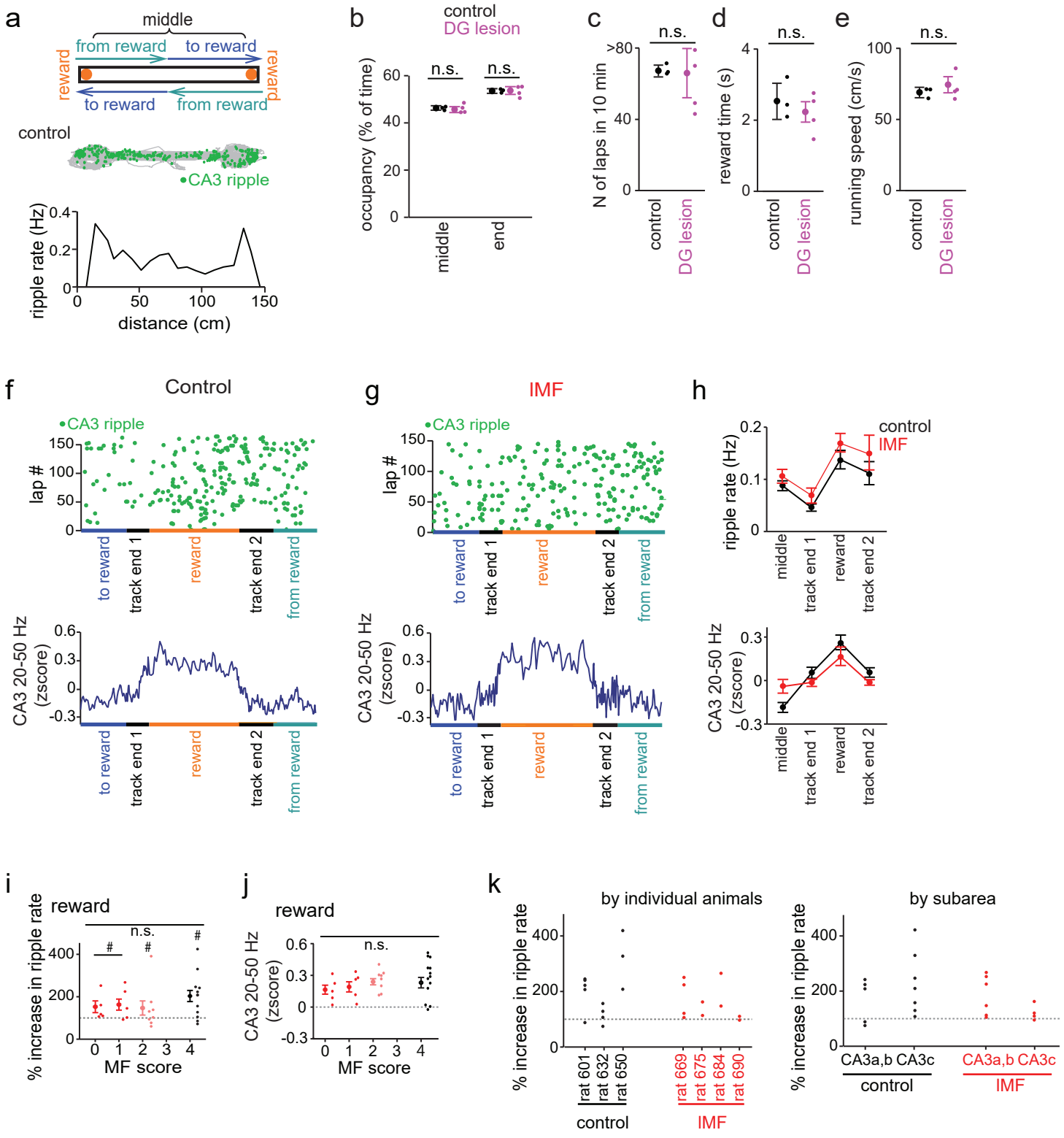

Supplementary Figure 13 CA3 ripple events during the linear track task were less dependent on MF input than in WM. (**a**) (From top to bottom) Schematic of behavioral phases on the linear track, ripple locations (green dots) during an example session on the linear track, and average ripple rates during the example session. Recordings were from a representative CA3 recording site in a control animal. (**b-e**) Motor performance in the linear track task did not differ between control and DG-lesioned animals. (**b**) Relative occupancy time in the middle and at the end of the track [n = 3 control and 4 lesioned animals; middle, t(5) = 0.07, P = 0.95; end t(5) = 0.07, P = 0.95, two-sided t test]. (**c**) Mean number of laps in a 10-min session [t(5) = 0.13, P = 0.90]. (**d**) Mean duration of reward consumption [t(5) = 0.74, P = 0.49, t test]. (**e**) Mean running speed on the track [t(5) = 0.66, P = 0.54, two-sided t test]. Bars are SEM. (**f**) CA3 ripples in a control rat. (Top) Rastergram depicts the distribution of ripple events during an example session on the linear track. For visualization of the distribution over multiple runs along the track, each behavioral period within a run was normalized to the average duration of the corresponding behavioral period [color coded as defined in (a), top schematic]. In addition, the period on the arm end was divided into the time before, during, and after reward consumption (track end 1, reward, and track end 2, respectively). (Bottom) Corresponding behavior-related CA3 20-50 Hz LFP power. (**g**) Same as (f) but for a site with low-density MF input (lMF) from a DG-lesioned rat. (**h**) (Top) Average frequency of behavior-related CA3 ripple events for control sites (black, n = 12 TT from 3 animals) and lMF (red, n = 10 TT from 4 animals) sites. From/to reward journeys are combined and reported as middle. No significant differences were found between the two types of recording sites [F(1,60) = 3.51, P = 0.076]. (Bottom) Average 20-50 Hz LFP power for control (black) and lMF (red) sites. At both types of sites, the power was increased during reward consumption and no significant difference was found between the two groups [F(1,60) = 0.75, P = 0.40; repeated measures ANOVA]. Bars are SEM. (**i**) Normalized ripple event rates for CA3 recording sites (compared to ripple rates during immobility before reward consumption). Individual sites (small circles with similar values jittered along the horizontal axis for visualization) and means (± SEM), grouped by the MF score, are shown. There was an increase in ripple rates during reward at control CA3 sites and at CA3 sites with hMF and lMF input [score 0: n = 5 TT from 3 animals, score 1: n = 5 TT from 3 animals, score 2: n = 8 TT from 3 animals, score 4, control: n = 12 TT from 3 animals; control: t(11) = 4.17, P = 0.0016; hMF: t(7) = 2.69, P = 0.031; lMF t(9) = 2.45, P = 0.037]. The percent increase in ripple rates did not differ between recording sites with varying degrees of MF innervation (control vs lMF, U = 148, Z = 0.62, P = 0.53; control vs hMF, U = 145, Z = 1.42, P = 0.15, two-sided Mann-Whitney U test followed by posthoc Bonferroni corrections), which is in contrast to the differences in ripple rates during WM performance (shown in **Fig. 4e**). (**j**) For each recording site, 20-50 Hz power during reward consumption was normalized to the average 20-50 Hz power outside the reward period. There was an increase in 20-50 Hz power during reward at control CA3 sites and at CA3 sites with hMF and lMF input [control: t(11) = 6.88, $P = 2.7 \times 10^{-5}$; hMF: t(7) = 6.63, $P = 3.0 \times 10^{-4}$; lMF t(9) = 5.84, $P = 2.4 \times 10^{-4}$, two-sided t test vs zero]. The percent increase in CA3 20-50 Hz power did not differ between recording sites with varying degrees of MF innervation ($P > 0.05$, comparison across groups), which is in contrast to the differences in 20-50 Hz power during WM performance (shown in **Fig. 5i**). (**k**) Same as in **Supplementary Fig. 11** but plotted for the linear track task. For each CA3 recording site, the ripple rate during reward consumption was normalized to the ripple rate when the animal had stopped at the track end. For visualization, data points with similar values were jittered along the horizontal axis.

Supplementary Figure 14

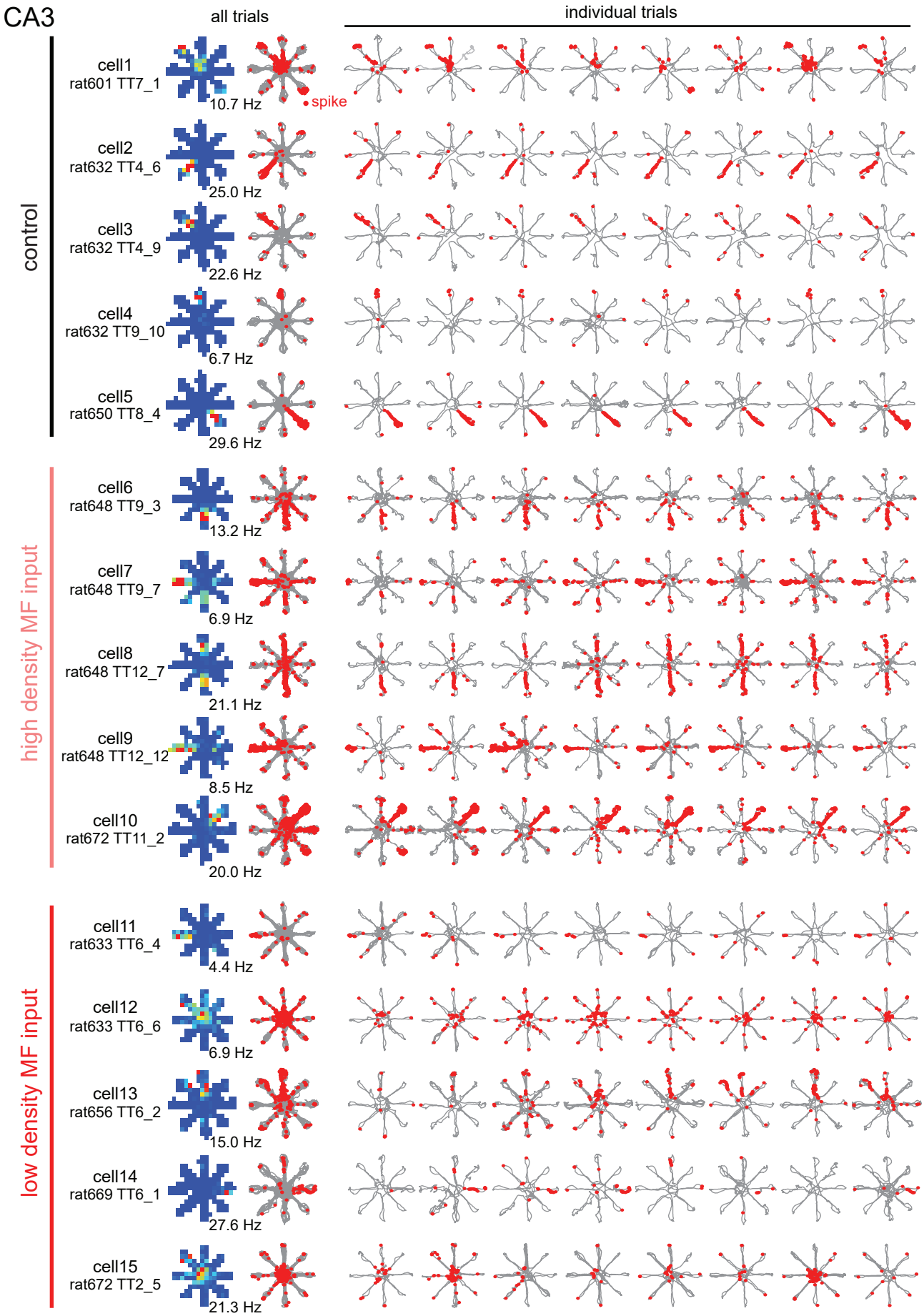

Supplementary Figure 14 Examples of place-specific firing of CA3 pyramidal cells in the spatial working memory task. Each row is the activity pattern of a single CA3 neuron. For each neuron, the rate map for the entire recording session is color-coded (blue, no firing; red, peak firing rate), and the trajectories (gray) with spike locations (red dots) are shown for all trials in a recording session and for the first 8 out of up to 20 individual trials (from left to right). The peak firing rate for each cell is listed in the lower-right corner of the rate map (in Hz). Neurons are separated into three groups: control, CA3 neurons at sites with high-density MF input (hMF), and CA3 neurons at sites with low-density or no MF input (lMF). Five representative CA3 neurons are shown for each group (total cells isolated: control, n = 116 cells from 4 animals; hMF, n = 49 cells from 5 animals; lMF, n = 57 cells from 9 animals).

Supplementary Figure 15

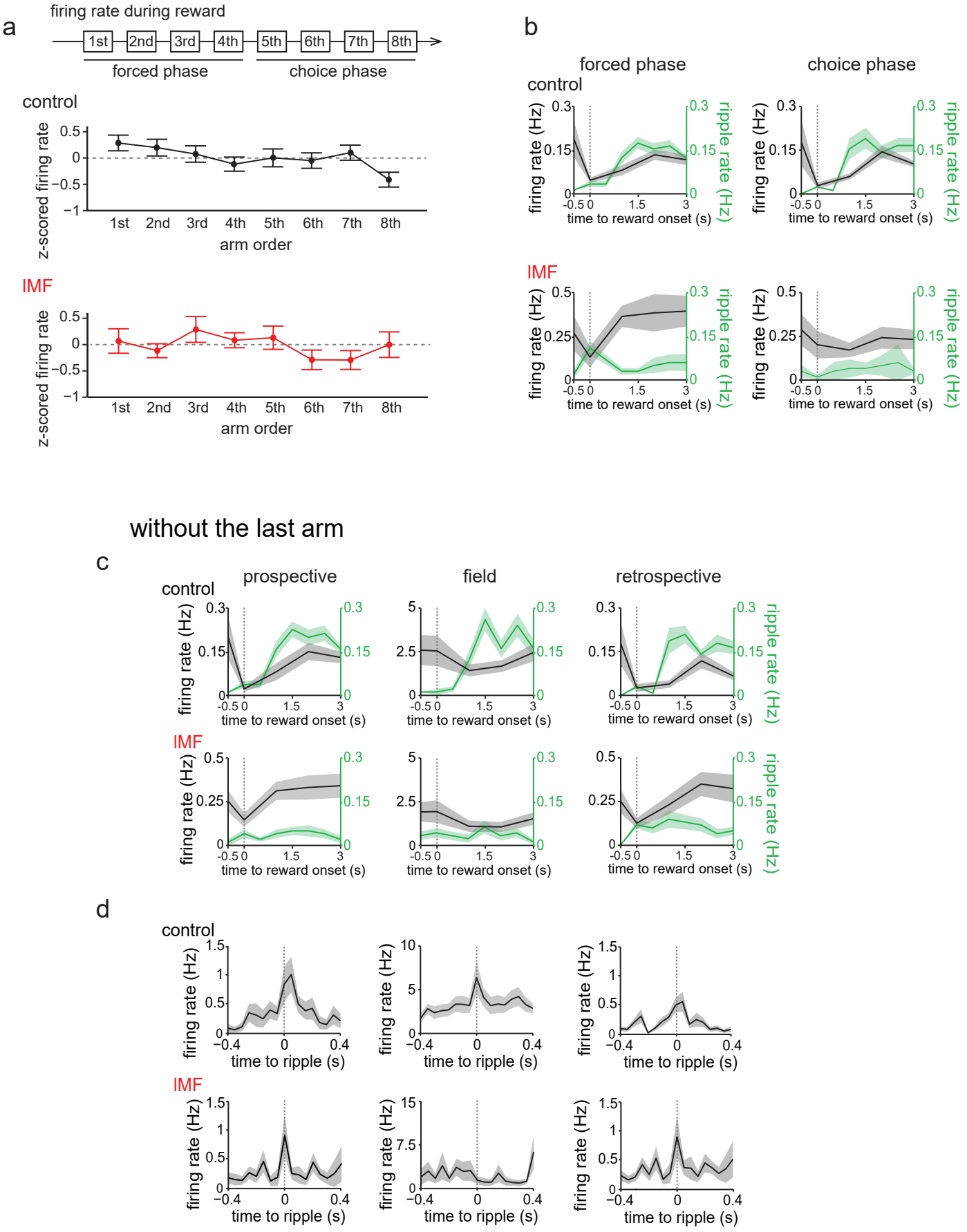

Supplementary Figure 15 Changes in CA3 reward-associated firing rates with behavior. (**a**) Firing rates of CA3 cells during reward consumption in the 1st to the 8th arm are shown as z-scores. Consistent with prospective firing patterns, control animals show a tendency for increased firing rates during earlier arm entries [n = 39 and 22 cells in 4 control and 9 lMF animals, respectively; control: F(7,266) = 1.82, P = 0.083, repeated measures ANOVA; lMF input: F(7,147) = 0.94, P = 0.48; control vs low-density MF input, F(1,413) = 0.40, P = 0.50]. Dashed lines denote 0. (**b**) Comparison of reward-associated ripple events between forced and choice phases. Time changes in firing rates of CA3 cells were aligned to the onset of reward consumption during both phases of behavior. The data are presented as described in **Fig. 7d**. Action potentials on arms with a cell's place field were excluded from the analysis. No significant differences between forced and choice phases were found when comparing the extent of firing rate changes during reward consumption (0-3 s, compared to period before reward) in either the control group [F(1,228) = 1.88, P = 0.17] or the lMF group [F(1,126) = 2.27, P = 0.14, repeated-measures ANOVA]. Moreover, no significant differences between forced and choice phases were found for the ripple rate change during reward in either group [control: F(1,456) = 0.77, P = 0.38; lMF: F(1,252) = 0.74, P = 0.39, repeated-measures ANOVA]. (**c,d**) Comparison of prospective and retrospective firing for the 1st to 7th arms visited within a trial. (**c**) Reward-related firing rates of CA3 cells for arm entries before (prospective), while (field), and after (retrospective) visiting the arm with their respective place fields. The data are presented as described in **Fig. 7d** with the exception that activity observed at the last arm in each trial were excluded from the analysis. Corresponding ripple event rates are shown in green. There was a significant difference between prospective and retrospective CA3 firing (gray) during reward consumption (0-3 s after the reward onset) in the control group [F(1,228) = 5.33, P = 0.024] but not the lMF group [F(1,126) = 0, P = 0.99], but there was no change in the ripple rate during reward consumption between prospective and retrospective periods [control: F(1,456) = 3.27, P = 0.075; lMF: F(1,252) = 1.28, P = 0.26, repeated-measures ANOVA]. (**d**) CA3 ripple-triggered firing rate changes. The data are presented as described in **Fig. 7e** but without the inclusion of activity from the last arm in the sequence. There was a significant difference between prospective and retrospective CA3 firing during ripples (0-150 ms after the ripple onset) in the control group [F(1,228) = 5.62, P = 0.020] but not the lMF group [F(1,126) = 0.14, P = 0.71, repeated-measures ANOVA]. Data excluding the last arm in the behavioral sequence support the data presented in **Fig. 7** in which neuronal activity patterns and oscillations from the last arm were included. Symbols with bars in (a) and lines with shaded area in (b-d) are mean ± SEM.

Supplementary Figure 16

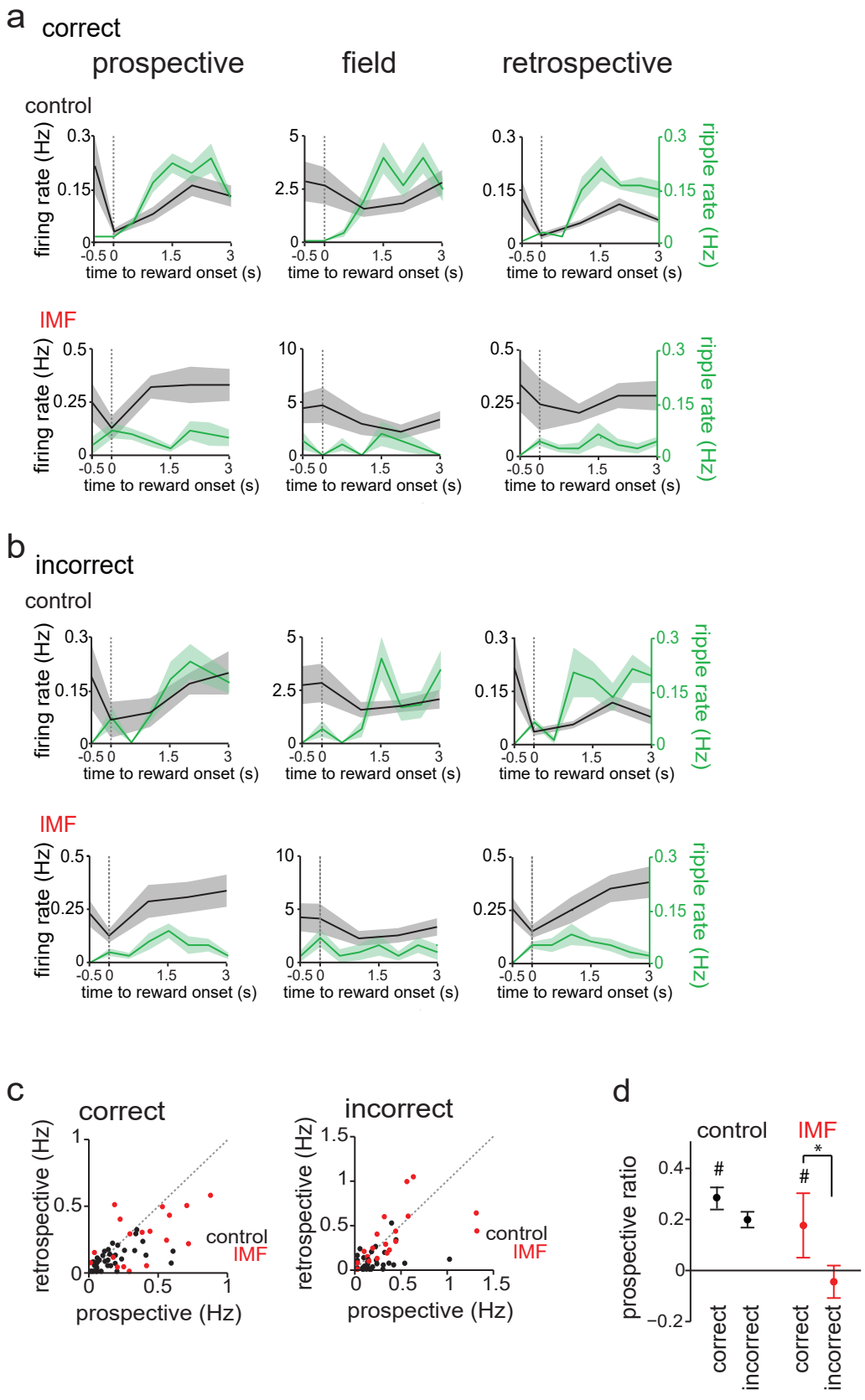

Supplementary Figure 16 Prospective firing at CA3 recording sites was observed in correct but not incorrect trials. (**a**) Reward-related firing rates of CA3 cells (gray) and corresponding ripple event rates (green) for arm entries before (prospective), while (field), and after (retrospective) visiting the arm with the place field. Only correct trials are included, and data are presented as described in **Fig. 7d**. There was a significant difference between prospective and retrospective CA3 firing during reward consumption (0-3 s after the reward onset) in the control group [$n = 39$ cells from 4 animals; $F(1,228) = 4.47$, $P = 0.038$) but not the lMF group ($n = 21$ cells from 5 animals; $F(1,120) = 0.41$, $P = 0.53$]. No differences were found in ripple rates between prospective and retrospective periods [control: $F(1,456) = 0.05$, $P = 0.82$; lMF: $F(1,240) = 1.77$, $P = 0.19$]. (**b**) Only incorrect trials were analyzed as in (a). No significant differences in the firing rate change and ripple rates were found between prospective and retrospective periods in either group [firing rate, control: $F(1,228) = 3.40$, $P = 0.069$; lMF: $F(1,120) = 0.03$, $P = 0.90$; ripple rate, control: $F(1,456) = 0.55$, $P = 0.46$; lMF: $F(1,240) = 0.08$, $P = 0.78$]. (**c**) Prospective and retrospective CA3 firing rates during reward consumption are shown separately for correct and incorrect trials (data are presented as described **Fig. 7f**). (**d**) In both control and lMF groups, prospective ratios were different from zero in correct trials, but not in incorrect trials [control (correct), $t(38) = 3.87$, $P = 4.2 \times 10^{-4}$; control (incorrect), $t(38) = 1.69$, $P = 0.10$; lMF (correct), $t(20) = 2.96$, $P = 0.0078$; lMF (incorrect), $t(20) = 0.61$, $P = 0.55$]. However, the difference between correct and incorrect trials reached significance in only the lMF but not in the control group [control, $t(38) = 0.85$, $P = 0.40$; lMF, $t(20) = 3.15$, $P = 0.005$, two-sided paired *t* test]. Along with the overall decrease in prospective coding in DG-lesioned rats (**Fig. 7f**), these data therefore indicate that DG lesions result in a reduced likelihood that upcoming goals are overrepresented. If prospective coding is relevant to behavior, it would thus result in the observed behavioral deficit (**Supplementary Fig. 1b** and **10b**), but it would also be expected that trials are more likely correct when prospective coding occasionally reemerges in the DG-lesioned rats, as shown in our data. # $P < 0.05$, *t* test vs. zero, * $P < 0.05$, two-sided paired *t* test. Lines with shaded regions in (a-b) and symbols with bars in (d) are mean ± SEM.

Supplementary Figure 17

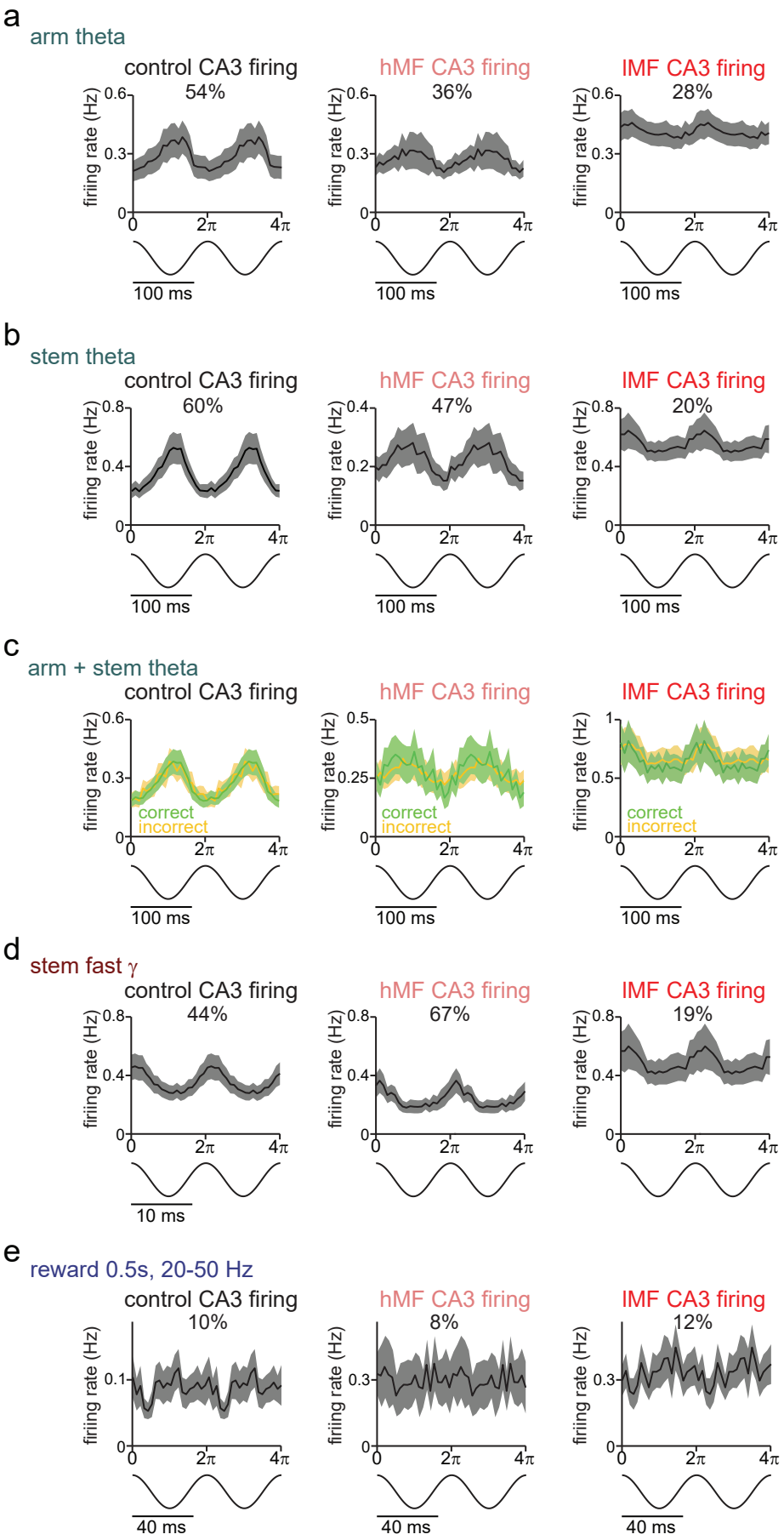

Supplementary Figure 17 Spike-rate distributions of CA3 principal cells across phases of theta and gamma oscillations. (**a,b**) Firing rates of CA3 pyramidal cells were plotted against the phase of theta (8-Hz) oscillations when the animals explored the arm (a) or the stem (b) of the radial maze during working memory performance. Data are separated by MF input (from left to right; control CA3 recording sites; DG-lesioned with high-density MF input, hMF; and DG-lesioned with low-density or no MF input, lMF). At the top of each graph the percentage of neurons that fired time-locked to the oscillatory cycle is indicated. The percentage of phase locked neurons was higher in the control group, compared with the hMF and lMF groups (control, n = 116 cells from 4 animals; hMF, n = 49 cells from 5 animals; lMF, n = 57 cells from 9 animals). (**c**) Theta-phase locking of CA3 neurons on the stem and arm combined, but now separated by correct (green) and incorrect (yellow) trials. There is no significant difference in the degree of phase locking between the two trial types [n = 116, 49, and 57 cells in control, hMF, and lMF groups, respectively; control: $F(1,8892) = 0$, $P = 0.96$; hMF: $F(1,3276) = 0.01$, $P = 0.93$; lMF: $F(1,3666) = 0.02$, $P = 0.88$, repeated-measures ANOVA] suggesting that theta-phase locking is not directly relevant to correct behavioral performance in the working memory task. (**d**) Same as in (a) but plotted against the phase of fast gamma (80-Hz) oscillations when animals were located on the stem of the maze. (**e**) Same as in (a) but plotted against the phase of the 20-50 Hz oscillation during the first 0.5 s of reward consumption. Consistent with the extremely low firing rates during this phase of behavior, entrainment of neuronal activity to the oscillation was not detected. Lines with shaded regions in (a-e) indicate the mean ± SEM.